2010 IEEE International Conference on Robotics and Automation
Anchorage Convention District
May 3-8, 2010, Anchorage, Alaska, USA

Reach then see: a new adaptive controller for robot manipulator based on dual task-space information

C.C. Cheah and X. Li
School of Electrical and Electronic Engineering
Nanyang Technological University
Block S1, Nanyang Avenue, S(639798)
Republic of Singapore

***Abstract*— It is interesting to observe from human visually guided tasks that visual feedback is not used for the entire movement, but only at end phases when our hand is near the target. We are able to move our hand from an initial position that is not within our field of view and transit smoothly and easily into visual feedback when the target is near. Inspired by this natural action, this paper presents a new task-space adaptive controller with dual feedback information. The proposed controller consists of a Cartesian-space region reaching controller at the initial stage and a vision based tracking controller that is only activated when the end effector enters an image region. A new potential energy function is proposed such that the image region can be fixed as the field of view of the camera and does not have to vary with the desired trajectory. The proposed task-space controller can transit smoothly from Cartesian-space reaching to vision-space tracking control. The stability of the closed-loop system is analyzed with consideration of the nonlinear dynamics. The proposed adaptive controller is implemented on an industrial robot and experimental results are presented to illustrate the performance of the proposed controller.**

I. INTRODUCTION

In conventional task-space control of robot, a single task-space information in either Cartesian space or visual space is used for the entire task. The basic idea of task-space control is to formulate a control scheme using the Cartesian error or visual error directly to eliminate the requirement of solving the inverse kinematics. The first Cartesian-space regulator was proposed by Takegaki and Arimoto [1]. It was shown using Lyapunov's method that the PD control plus gravity compensation is effective for setpoint control despite the nonlinearity and uncertainty of the robot dynamics. Inspired by the original work [1], much progress has been achieved in understanding the task-space regulation problems [2]–[5]. To deal with trajectory tracking control, Slotine and Li [6] proposed a Cartesian-space adaptive controller. Most researches on robot control have assumed that the exact kinematics and Jacobian matrix of the manipulator are known. To overcome the problem of uncertain kinematics, Cheah *et al.* [7] presented an adaptive Jacobian tracking controller with concurrent adaptation to both kinematics and dynamic uncertainties. Recently, the problems of depth uncertainty in image based control have been studied in [8], [9].

However, those aforementioned task-space controllers use only single task-space information for the entire task, which is either defined in Cartesian space [1], [6] or in image space [7], [8]. Visual feedback control is robust to modeling and calibration errors and also improves the accuracy of end-point positioning [10]. However, if image information is used for the entire task, the camera may not be able to cover the entire workspace because of a limited field of view. In addition, when the end-effector moves at a high speed, it is difficult to track the image feature.

It is interesting to observe in human reaching movement that the visual feedback is not used for the entire movement, but only at end phases when our hand is near the target. We are able to move our hand from an initial position that is not within our field of view and transit smoothly and easily into visual feedback when the target is near. The exploration of a controller that mimic such human behavior is an important step toward understanding dextrous movement of robot. Recently, a new task-space control strategy that allows the use of dual task-space information for a single controller is proposed [11]. The task-space setpoint controller only requires vision feedback when the end effector is near the desired position. However, the result in [11] is focusing on setpoint control or point-to-point control of robot. In addition, the desired position must be defined as the geometrical center of the image region and therefore the image region varies with the desired position and hence can not be fixed as the camera's field of views.

In this paper, we propose a new task-space adaptive controller. The main contribution is the development of a new potential energy function such that its geometrical center is not necessary the desired motion. Therefore, the image region can be fixed as the field of view of the camera and does not have to vary with the desired trajectory. In addition, the task-space controller only requires vision feedback when the end-effector is near the desired trajectory. The proposed controller consists of a Cartesian-space region reaching controller that is activated at the initial stages and a vision based tracking controller that is only activated when the end effector enters the image region. The proposed task-space controller can transit smoothly from Cartesian-space reaching to vision-space tracking control. The proposed adaptive controller is implemented on an industrial robot and experimental results are presented to illustrate the performance of the controller.

978-1-4244-5040-4/10/$26.00 ©2010 IEEE

II. ROBOT KINEMATICS AND DYNAMICS

We consider a robot system with camera(s) fixed in the work space. Let $r \in \Re^p$ denotes a position of the end effector in Cartesian space as [3] [12]:

$$r = h(q), \tag{1}$$

where $h(\cdot) \in \Re^n \rightarrow \Re^p$ is generally a non-linear transformation describing the relation between joint space and task space, $q = [q_1, \cdots, q_n]^T \in \Re^n$ is a vector of joint angles of the manipulator. The velocity of the end-effector $\dot{r}$ is related to joint-space velocity $\dot{q}$ as:

$$\dot{r} = J_m(q)\dot{q}, \tag{2}$$

where $J_m(q) \in \Re^{p \times n}$ is the Jacobian matrix from joint space to task space.

For a visual servoing system, cameras are used to observe the position of the end-effector in image space. We use the standard pinhole camera model for the mapping from Cartesian space to image space, which has been proven adequate for most visual servoing tasks [10]. Let $x_i = [x_{hi}, x_{vi}]^T \in \Re^2$ denotes a feature point, while x_{hi} represents the horizontal coordinate and x_{vi} the vertical coordinate. Then $x = [x_1, x_2, \cdots, x_i, \cdots, x_m]^T \in \Re^{2m}$ denotes a vector of image features, where m is the number of image features. The relationship between rate of the change of the image features and the velocity of end-effector is represented by an image Jacobian matrix $J_I(r)$ as [13] [14]:

$$\dot{x} = J_I(r)\dot{r}. \tag{3}$$

From equations (2) and (3), we have:

$$\dot{x} = J_I(r)J_m(q)\dot{q} = J(q)\dot{q}, \tag{4}$$

where $J(q) \in \Re^{2m \times n}$ is the Jacobian matrix mapping from joint space to image space.

The dynamics of manipulator is described by [3] [12]:

$$M(q)\ddot{q} + (\frac{1}{2}\dot{M}(q) + S(q,\dot{q}))\dot{q} + g(q) = \tau, \tag{5}$$

where $M(q) \in \Re^{n \times n}$ is an inertia matrix, $g(q) \in \Re^n$ denotes the gravity vector, $\tau \in \Re^n$ denotes the control inputs, and

$$S(q,\dot{q})\dot{q} = \frac{1}{2}\dot{M}(q)\dot{q} - \frac{1}{2}\{\frac{\partial}{\partial q}\dot{q}^T M(q)\dot{q}\}^T.$$

Three important properties of the robot dynamics described by equation (5) are given as follows [3] [12]:

Property 1: The inertia matrix $M(q)$ is symmetric and positive definite for all $q \in \Re^n$.

Property 2: The matrix $S(q,\dot{q})$ is skew-symmetric such that:

$$y^T S(q,\dot{q})y = 0, \tag{6}$$

for any $y \in \Re^n$.

Property 3: The dynamic model as described by equation (5) is linear in a set of physical parameters $\theta_d = (\theta_{d1}, \cdots, \theta_{dp})^T$:

$$M(q)\ddot{q} + (\frac{1}{2}\dot{M}(q) + S(q,\dot{q}))\dot{q} + g(q) = Y_d(q,\dot{q},\dot{q},\ddot{q})\theta_d, \tag{7}$$

where $Y_d(q,\dot{q},\dot{q},\ddot{q}) \in \Re^{n \times p}$ is called the dynamic regressor.

III. TASK-SPACE ADAPTIVE TRACKING CONTROL WITH DUAL TASK-SPACE INFORMATION

In this section, we present the proposed task-space tracking controller with dual feedback signals. The basic idea is to divide the task into two regions: a Cartesian-space region for the reaching movement of robot's end-effector at the beginning stage and an image-space region for the tracking control task at the end stage.

Let $x_{di}(t) = [x_{dhi}(t), x_{dvi}(t)]^T \in \Re^2$ denotes a desired trajectory of the i^{th} feature in the image region. We define the image region as follows:

$$f_i(\Delta x_i) = \frac{(x_{hi}(t) - x_{dhi}(t))^N}{(x_{bhi} - x_{dhi}(t))^N} + \frac{(x_{vi}(t) - x_{dvi}(t))^N}{(x_{bvi} - x_{dvi}(t))^N} - 1 \leq 0, \tag{8}$$

where $x_{bi} = [x_{bhi}, x_{bvi}]^T \in \Re^2$ represents the fixed boundary of the region, and $\Delta x_i = x_i(t) - x_{di}(t)$ denotes the image error. The image region $f_i(\Delta x_i) \leq 0$ denotes a superellipse region with order N, where N is an even integer.

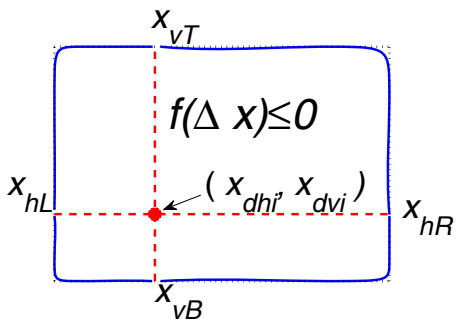

Fig. 1. Example of the image region $f_i(\Delta x_i) \leq 0$ with $N = 20$

The desired trajectory $x_{di}(t)$ is specified within the image region, and the image region is divided into four parts with respect to $x_{di}(t)$, as illustrated in Figure 1. From Figure 1, the boundary of image region is defined by four parameters: x_{hR}, x_{hL}, x_{vT} and x_{vB}. Hence the boundary positions in equation (8) are set as:

$$x_{bhi} = \begin{cases} x_{hL}, & x_{hi} \leq x_{dhi}, \\ x_{hR}, & x_{hi} > x_{dhi}, \end{cases} \tag{9}$$

$$x_{bvi} = \begin{cases} x_{vB}, & x_{vi} \leq x_{dvi}, \\ x_{vT}, & x_{vi} > x_{dvi}. \end{cases} \tag{10}$$

Using the image region function (8), a potential energy function is specified in image space as:

$$P_i(x_i) = \frac{a_i}{2}(1 - [min(0, f_i(\Delta x_i))]^2), \tag{11}$$

where a_i are positive constants.

Note that when the order N in equation (8) varies, $f_i(\Delta x_i)$ and $P_i(x_i)$ also change. Let $f_{li}(\Delta x_i)$ be a lower order function of (8) with order N_l (e.g. $N_l = 2$) and $f_{hi}(\Delta x_i)$ be a higher order function with order N_h (e.g. $N_h = 20$), where N_l and N_h are both even integers. Using $f_{li}(\Delta x_i)$ and $f_{hi}(\Delta x_i)$ in equation (11), we obtain a low-order potential energy $P_{li}(x_i)$ and a high-order potential energy $P_{hi}(x_i)$ respectively, which are shown in Figure 2 and 3.

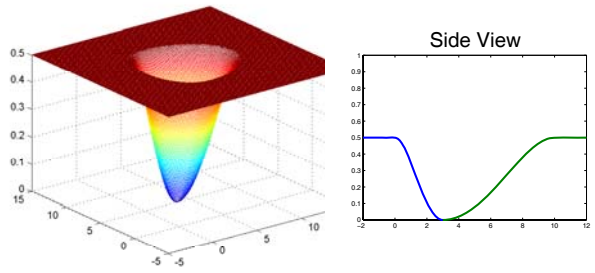

Fig. 2. A low-order potential energy $P_{li}(x_i)$ with $N_l = 2$

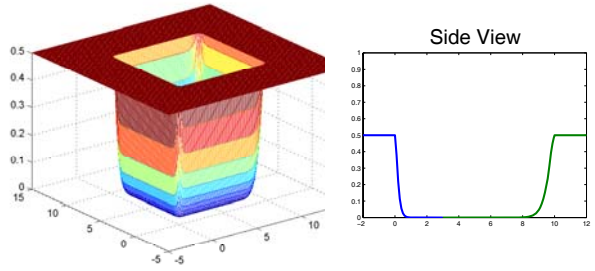

Fig. 3. A high-order potential energy $P_{hi}(x_i)$ with $N_h = 20$

From Figure 2 and Figure 3, it is observed that when the order of the function (8) is high, the bottom part of the potential energy becomes flat, while the top contour is close to a rectangle. When the order is low, the bottom part of the potential energy is a point, but the top contour is not a rectangle and therefore can not cover a large image space. Combining the advantages of the low-order and the high-order functions, the overall potential energy is proposed as:

$$P_{ci}(x_i) = P_{hi}(x_i) + P_{li}(x_i). \tag{12}$$

The overall potential energy is illustrated in Figure 4. It is interesting to observe that with different $x_{di}(t)$, the top contours of overall potential energy remain the same while the bottom part of the potential energy varies (see Figure 4).

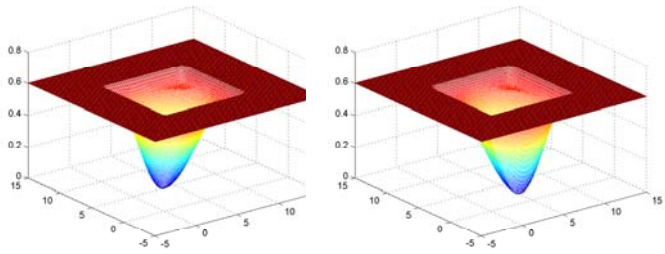

Fig. 4. Overall image potential energy $P_{ci}(x_i)$ with different $x_{di}(t)$

In the presence of multiple features, the image regions can be specified as:

$$f_h(\Delta x) = [f_{h1}(\Delta x_1), f_{h2}(\Delta x_2), \cdots, f_{hm}(\Delta x_m)]^T \leq 0,$$

$$f_l(\Delta x) = [f_{l1}(\Delta x_1), f_{l2}(\Delta x_2), \cdots, f_{lm}(\Delta x_m)]^T \leq 0.$$

Therefore, the overall potential energy is given in image space as:

$$\begin{aligned} P_c(x) &= \textstyle\sum_{i=1}^m P_{ci}(x_i) = \sum_{i=1}^m P_{hi}(x_i) + \sum_{i=1}^m P_{li}(x_i) \\ &= k_p\alpha_x \textstyle\sum_{i=1}^m \frac{a_{hi}}{2}(1 - [min(0, f_{hi}(\Delta x_i))]^2) \\ &\quad + k_p\alpha_x \textstyle\sum_{i=1}^m \frac{a_{li}}{2}(1 - [min(0, f_{li}(\Delta x_i))]^2), \end{aligned} \tag{13}$$

where a_{hi}, a_{li}, α_x and k_p are positive constants. Note that $P_c(x)$ is also lower bounded by zero.

Partial differentiating the potential energy functions in equations (13) with respect to Δx, we have:

$$\begin{aligned} &\textstyle\sum_{i=1}^m (\frac{\partial P_{hi}(x_i)}{\partial \Delta x})^T \\ &= -k_p\alpha_x \textstyle\sum_{i=1}^m a_{hi} min(0, f_{hi}(\Delta x_i))(\frac{\partial f_{hi}(\Delta x_i)}{\partial \Delta x})^T, \end{aligned} \tag{14}$$

$$\begin{aligned} &\textstyle\sum_{i=1}^m (\frac{\partial P_{li}(x_i)}{\partial \Delta x})^T \\ &= -k_p\alpha_x \textstyle\sum_{i=1}^m a_{li} min(0, f_{li}(\Delta x_i))(\frac{\partial f_{li}(\Delta x_i)}{\partial \Delta x})^T. \end{aligned} \tag{15}$$

Based on equations (14) and (15), we define two region errors as:

$$\Delta\xi_h = \sum_{i=1}^m a_{hi} min(0, f_{hi}(\Delta x_i))(\frac{\partial f_{hi}(\Delta x_i)}{\partial \Delta x})^T, \tag{16}$$

$$\Delta\xi_l = \sum_{i=1}^m a_{li} min(0, f_{li}(\Delta x_i))(\frac{\partial f_{li}(\Delta x_i)}{\partial \Delta x})^T. \tag{17}$$

As seen from equation (11) and Figure 4, there is no change in potential energy with respect to position when $x(t)$ is outside the image region. Hence, the image region errors $\Delta\xi_h$ and $\Delta\xi_l$ are zero when $x(t)$ is outside image region (i.e. $f_h(\Delta x) > 0$ and $f_l(\Delta x) > 0$). When the end-effector enters the image region, they become nonzero.

Next, a Cartesian region is defined as:

$$\begin{aligned} f_1(r_1) &= \tfrac{(r_1 - r_{c1})^2}{(r_{b1} - r_{c1})^2} - 1 \leq 0, \\ &\cdots \\ f_p(r_p) &= \tfrac{(r_p - r_{cp})^2}{(r_{bp} - r_{cp})^2} - 1 \leq 0, \end{aligned} \tag{18}$$

where $r = [r_1, \cdots, r_p]^T \in \Re^p$ denotes the position of end-effector in Cartesian space. Since the objective is to bring the end-effector into the image region, only position of the end-effector is sufficient and therefore p is usually less than 3. The vector $r_b = [r_{b1}, \cdots, r_{bp}]^T \in \Re^p$ represents boundary position in individual coordinate, and the vector $r_c = [r_{c1}, \cdots, r_{cp}]^T \in \Re^p$ denotes a reference point within Cartesian region. The Cartesian region is constituted by several sub-regions. Other examples of region can be referred in [16].

The total potential energy in Cartesian space is defined as:

$$P_r(r) = \sum_{i=1}^p P_i(r_i) = \sum_{i=1}^p \frac{k_p\alpha_r}{2}[max(0, f_i(r_i))]^2, \tag{19}$$

where k_p and α_r are positive constants. An illustration of the above function is shown in Figure 5.

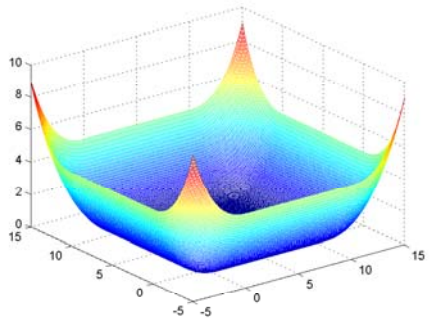

Fig. 5. A potential energy $P_r(r)$ in 2-D Cartesian space

Partial differentiating the above potential energy function (19) with respect to r, we have:

$$\frac{\partial P_r(r)}{\partial r} = k_p \alpha_r \sum_{i=1}^{p} max(0, f_i(r_i))(\frac{\partial f_i(r_i)}{\partial r})^T. \quad (20)$$

From the definition of Cartesian region function, note that $\sum_{i=1}^{p} max(0, f_i(r_i))(\frac{\partial f_i(r_i)}{\partial r})^T \neq 0$ when end-effector is outside the Cartesian region. Once the end-effector reaches the region, this term becomes zero. This is the crucial difference between the image region control and the Cartesian region control.

Next we define a region error in Cartesian space as:

$$\Delta\varepsilon_r = \sum_{i=1}^{p} max(0, f_i(r_i))(\frac{\partial f_i(r_i)}{\partial r})^T. \quad (21)$$

Since visual feedback is only used when the end-effector reaches the image-space region, the desired trajectory in image space is specified so that:

$$\dot{x}_d = \begin{cases} 0, & \Delta\varepsilon_r \neq 0, \\ \dot{x}_d(t), & \Delta\varepsilon_r = 0. \end{cases} \quad (22)$$

Next, a reference vector is introduced as:

$$\dot{x}_{ai} = [\dot{x}_{dhi} - \dot{x}_{dhi}\frac{x_{hi} - x_{dhi}}{x_{bhi} - x_{dhi}}, \quad \dot{x}_{dvi} - \dot{x}_{dvi}\frac{x_{vi} - x_{dvi}}{x_{bvi} - x_{dvi}}]^T.$$

Let $\dot{x}_a = [\dot{x}_{a1}, \cdots, \dot{x}_{am}]^T \in \Re^{2m}$, a sliding vector is defined as

$$s = \dot{q} - \dot{q}_r = \dot{q} - J_m^+(q)J_I^+(r)\dot{x}_a$$
$$-\alpha_x J_m^+(q)J_I^T(r)(\Delta\xi_h + \Delta\xi_l) + \alpha_r J_m^+(q)\Delta\varepsilon_r, \quad (23)$$

where $J_m^+(q)$ is the pseudo-inverse matrix of $J_m(q)$, $J_I^+(r)$ is the pseudo-inverse matrix of $J_I(r)$ and $J_I^T(r)$ is the transpose matrix of $J_I(r)$.

The task-space tracking controller with dual feedback information and the dynamics update law are proposed as:

$$\tau = k_p \alpha_x J_m^T(q)J_I^T(r)(\Delta\xi_h + \Delta\xi_l)$$
$$-k_p \alpha_r J_m^T(q)\Delta\varepsilon_r - K_v s + Y_d(q, \dot{q}, \dot{q}_r, \ddot{q}_r)\hat{\theta}_d, \quad (24)$$

$$\dot{\hat{\theta}}_d = -L_d Y_d^T(q, \dot{q}, \dot{q}_r, \ddot{q}_r)s, \quad (25)$$

where $K_v \in \Re^{n \times n}$ is a positive definite matrix. L_d is a positive definite matrix and $\hat{\theta}_d$ is the vector of estimated dynamic parameters. The Cartesian region described by $f_r(r) \leq 0$ is slightly overlapped with the image region $f_h(\Delta x) \leq 0$, such that the gradient of the overall potential energy $P_c(x) + P_r(r)$ does not reduce to zero. Therefore, the first and second term on the right side of equation (24) do not reduce to zero at the same time during the transition from Cartesian space to image space.

Using equation (23), the robot dynamics is presented as:

$$M(q)\dot{s} + (\frac{1}{2}\dot{M}(q) + S(q, \dot{q}))s + Y_d(q, \dot{q}, \dot{q}_r, \ddot{q}_r)\theta_d = \tau. \quad (26)$$

Substituting the control law described by equation (24) into equation (26), we obtain the closed-loop equation as:

$$M(q)\dot{s} + (\tfrac{1}{2}\dot{M}(q) + S(q, \dot{q}))s$$
$$-k_p \alpha_x J_m^T(q)J_I^T(r)(\Delta\xi_h + \Delta\xi_l) + k_p \alpha_r J_m^T(q)\Delta\varepsilon_r$$
$$+K_v s + Y_d(q, \dot{q}, \dot{q}_r, \ddot{q}_r)\Delta\theta_d = 0. \quad (27)$$

A Lyapunov-like function is defined as

$$V = \frac{1}{2}s^T M(q)s + P_c(x) + P_r(r) + \frac{1}{2}\Delta\theta_d^T L_d^{-1}\Delta\theta_d. \quad (28)$$

Differentiating equation (28) respect to time, we get:

$$\dot{V} = s^T M(q)\dot{s} + \tfrac{1}{2}s^T \dot{M}(q)s$$
$$-k_p \alpha_x \textstyle\sum_{i=1}^{m} a_{hi} min(0, f_{hi}(\Delta x_i))(\dot{x} - \dot{x}_a)^T (\frac{\partial f_{hi}(\Delta x_i)}{\partial \Delta x})^T$$
$$-k_p \alpha_x \textstyle\sum_{i=1}^{m} a_{li} min(0, f_{li}(\Delta x_i))(\dot{x} - \dot{x}_a)^T (\frac{\partial f_{li}(\Delta x_i)}{\partial \Delta x})^T$$
$$+ \textstyle\sum_{i=1}^{p} k_p \alpha_r max(0, f_i(r_i))\dot{r}^T (\frac{\partial f_i(r_i)}{\partial r})^T$$
$$-\dot{\hat{\theta}}_d^T L_d^{-1}\Delta\theta_d. \quad (29)$$

Then substituting equation (22), (23), (25) and (27) into equation (29) and using Property 2, we obtain:

$$\dot{V} = -s^T K_v s$$
$$-k_p[\alpha_r \Delta\varepsilon_r - \alpha_x J_I^T(r)(\Delta\xi_h + \Delta\xi_l)]^T \times$$
$$[\alpha_r \Delta\varepsilon_r - \alpha_x J_I^T(r)(\Delta\xi_h + \Delta\xi_l)] \leq 0. \quad (30)$$

We can now state the following theorem:

Theorem : *The adaptive control law (24) and the parameter update law (25) for the robot system (5) guarantee the convergence of the tracking errors. That is* $x(t) \to x_d(t)$, $\dot{x}(t) \to \dot{x}_d(t)$ *as* $t \to \infty$.

Proof: Since $M(q)$ is uniformly positive definite, V in equation (28) is positive definite in s and $\Delta\theta_d$. Since $V > 0$ and $\dot{V} \leq 0$, V is bounded. Hence, s, $\Delta\theta_d$, $P_r(r)$ and $P_c(x)$ are bounded. Thus $f_i(\Delta x_i)$ and $f_i(r_i)$ are also bounded, and $\frac{\partial f_i(\Delta x_i)}{\partial \Delta x}$, $\frac{\partial^2 f_i(\Delta x_i)}{\partial \Delta x^2}$ and $\frac{\partial f_i(r_i)}{\partial r}$, $\frac{\partial^2 f_i(r_i)}{\partial r^2}$ are also bounded. Therefore, $(\Delta\xi_h + \Delta\xi_l)$ and $\Delta\varepsilon_r$ are bounded. Then from equation (23), q_r is also bounded. $\dot{q}$ in equation (23) is also bounded since s is bounded. The boundedness of $\dot{q}$ guarantees the boundedness of $\dot{x}$ and $\dot{r}$ since both $J_m(q)$ and $J_I(r)$ are trigonometric function. Since $\frac{\partial f_i(\Delta x_i)}{\partial \Delta x}$, $\frac{\partial^2 f_i(\Delta x_i)}{\partial \Delta x^2}$ and $\frac{\partial f_i(r_i)}{\partial r}$, $\frac{\partial^2 f_i(r_i)}{\partial r^2}$ are bounded, $(\Delta\dot{\xi}_h + \Delta\dot{\xi}_l)$ and $\Delta\dot{\varepsilon}_r$ are bounded. Then $\ddot{q}_r$ is bounded. From the closed-loop equation (27), we can conclude that $\dot{s}$ is bounded. Thus, $\ddot{q}$ is bounded since $\dot{s} = \ddot{q} - \ddot{q}_r$. Thus, $\dot{V}$ is bounded since $\dot{s}$, s, $(\Delta\dot{\xi}_h + \Delta\dot{\xi}_l)$, $(\Delta\xi_h + \Delta\xi_l)$, $\Delta\dot{\varepsilon}_r$, $\Delta\varepsilon_r$ are bounded.

Therefore, $\dot{V}$ is uniformly continuous. Applying Barbalat's lemma [15], we have $\dot{V} \to 0$ which also indicates:

$$(\alpha_r \Delta\varepsilon_r - \alpha_x J_I^T(r)(\Delta\xi_h + \Delta\xi_l)) \to 0, \qquad (31)$$

and $s \to 0$.

If the end-effector is located outside the image region, then $\Delta\varepsilon_r \neq 0$, $\Delta\xi_h = 0$ and $\Delta\xi_l = 0$, which contracts with equation (31). If the end-effector is located within the overlapped region, then $\Delta\varepsilon_r \neq 0$, $\Delta\xi_h \neq 0$ and $\Delta\xi_l \neq 0$. Since the gradient of overall potential energy is not zero, the end-effector can not settle down. Therefore, the end-effector can only settle down within the Cartesian region and image region. Then $\Delta\varepsilon_r = 0$ and from (31) $(\Delta\xi_h + \Delta\xi_l) = 0$.

Since N_h and N_l are both even integers, $N_h - 1$ and $N_l - 1$ are both odd integers. Therefore the signs of the pair of entry in $(\frac{\partial f_{hi}(\Delta x_i)}{\partial \Delta x})^T$ and $(\frac{\partial f_{li}(\Delta x_i)}{\partial \Delta x})^T$ are always the same. Then the signs of $\Delta\xi_h$ and $\Delta\xi_l$ in equation (16) and (17) are always the same. Hence $(\Delta\xi_h + \Delta\xi_l) = 0$ indicates that $\Delta\xi_h = 0$ and $\Delta\xi_l = 0$. From equation (16) and (17) only $(\frac{\partial f_{hi}(\Delta x_i)}{\partial \Delta x})^T = 0$ and $(\frac{\partial f_{li}(\Delta x_i)}{\partial \Delta x})^T = 0$ can ensure that $\Delta\xi_h$ and $\Delta\xi_l$ reduce to zero, which mean $\Delta x \to 0$ and $x(t) \to x_d(t)$ as $t \to \infty$. From the definition of s in equation (23), $x(t) \to x_d(t)$ and $\Delta\varepsilon_r \to 0$ indicate that $\dot{x}_a \to \dot{x}_d(t)$. Therefore, $s \to 0$ and $\dot{x}_a \to \dot{x}_d(t)$ implies $\dot{x}(t) \to \dot{x}_d(t)$ as $t \to \infty$. △△△

Remark: For $P_{li}(x_i)$, when $N_l > 2$ the bottom part becomes a flat area, hence $N_l = 2$ is usually chosen as the order of $P_{li}(x_i)$. For $P_{hi}(x_i)$, if N_h is too small, the top contour is not a rectangle and hence can not cover a large image region. Therefore, N_h is chosen larger than 20. From equation (8), note that the order of denominator is not less than that of numerator in $(\frac{\partial f_i(\Delta x_i)}{\partial x})^T$ and $f_i(\Delta x_i)$. When the end-effector starts from an initial position outside the image region, the region errors $\Delta\xi_h$ and $\Delta\xi_l$ are always zero regardless of the order. When the end-effector is inside the finite image region, the tracking error is also finite and hence the region errors are bounded.

IV. EXPERIMENT

The proposed adaptive tracking controller was implemented on an industrial robot. The experimental setup consists of a PSD camera: C5949 and a Sony SCARA robot. An end-effector is attached to the second joint of robot. The PSD camera is used to measure the position of end-effector in image space in the unit of voltage [17]. The image region is defined by a superellipse: $f_h(\Delta x) \leq 0$ with $N = 20$, and the size of the rectangle with smoothed corners is $0.13V \times 0.13V$. The order of $f_l(\Delta x) \leq 0$ is $N = 2$, and the Cartesian region is slightly overlapped with the image region. The control gains are set as: $a_{ph} = 0.01$, $a_{pl} = 0.1$, $K_v = 0.0001$, $\alpha_x = 0.001$, $\alpha_r = 3 \times 10^{-8}$, $k_p = 1000$ and $L_d = diag(0.01, 0.01)$.

In the first experiment, the desired trajectory is specified as:

$$\begin{cases} x_{dh} = -0.55 - 0.002(t - t_r)(1 - e^{-k(t-tr)}), \\ x_{dv} = \quad 0.71 - 0.002(t - t_r)(1 - e^{-k(t-tr)}), \end{cases}$$

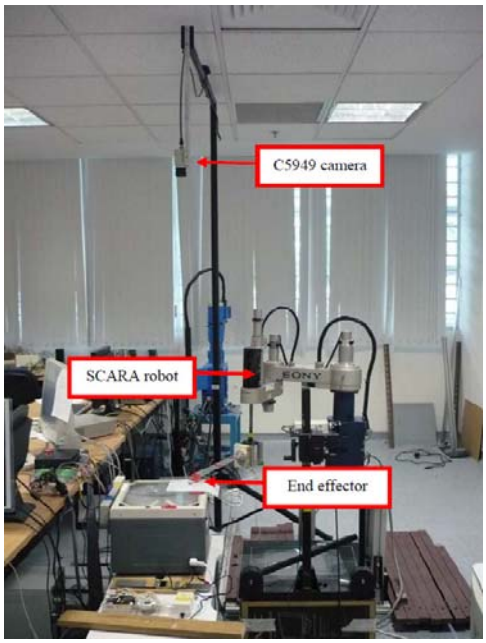

Fig. 6. Experimental setup

where t_r is the time taken for the end-effector to reach the Cartesian region, and k is a positive constant. The experimental results are shown in Figure 7 - Figure 9. t_v is the time when the end-effector enters the image region.

In the second experiment, the desired trajectory is specified as:

$$\begin{cases} x_{dh} = -0.57 + 0.026cos(12(t - t_r) + \pi)(1 - e^{-k(t-tr)}), \\ x_{dv} = \quad 0.69 + 0.028sin(12(t - t_r) + \pi)(1 - e^{-k(t-tr)}), \end{cases}$$

the experimental results are shown in Figure 10 - Figure 12.

V. CONCLUSION

In this paper, a new adaptive controller that allows the use of visual feedback at the end stage, has been presented. The proposed task-space controller can transit smoothly from Cartesian-space feedback at the initial stage to vision-space tracking control when the end effector enters the image region. Experimental results have been presented to illustrate the performance of the proposed controller.

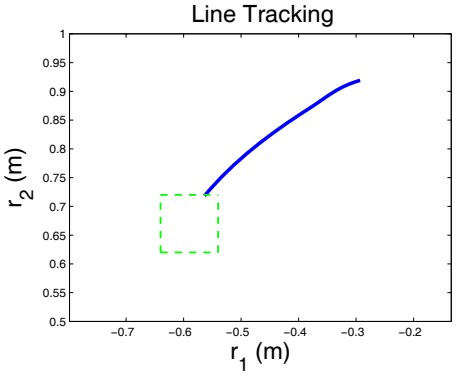

Fig. 7. Path of end-effector in Cartesian space (line tracking)

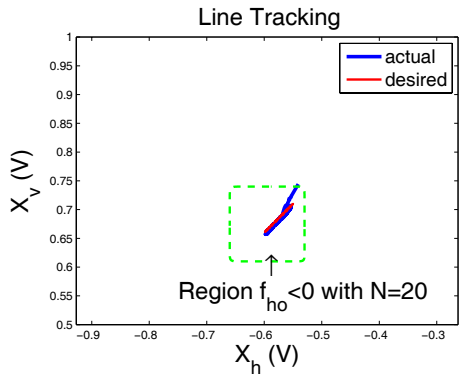

Fig. 8. Path of end-effector in image space (line tracking)

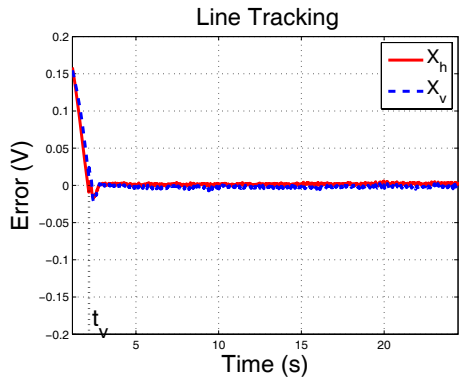

Fig. 9. Tracking errors (line tracking)

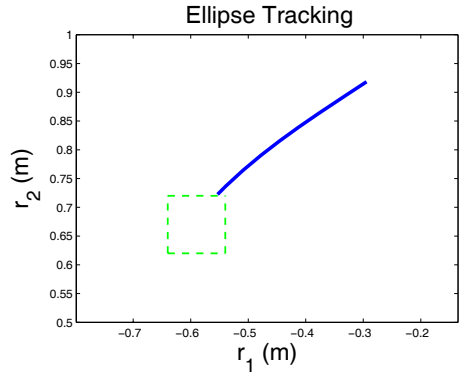

Fig. 10. Path of end-effector in Cartesian space (ellipse tracking)

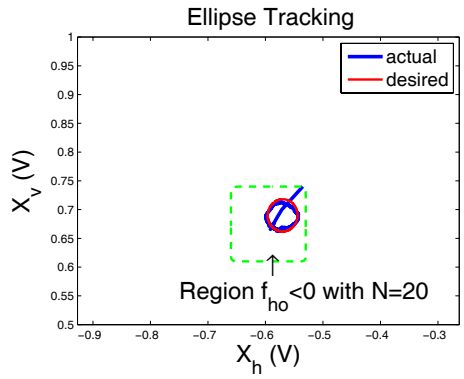

Fig. 11. Path of end-effector in image space (ellipse tracking)

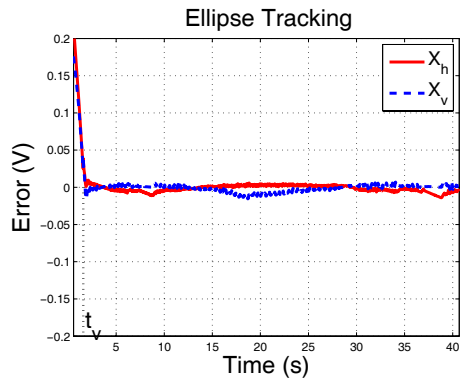

Fig. 12. Tracking errors (ellipse tracking)

REFERENCES

[1] M. Takegaki and S. Arimoto, "A new feedback method for dynamic control of manipulators," *ASME J. of Dynamic Systems, Measurement and Control*, Vol. 102, pp. 119-125, 1981.

[2] R. Kelly, "Regulation of manipulators in generic task space: An energy shaping plus damping injection approach," *IEEE Trans. on Robotics and Automation*, Vol. 15, pp. 381-386, 1999.

[3] S. Arimoto, *Control Theory of Non-Linear Mechanical Systems*. Oxford University Press, 1996.

[4] S. Arimoto and F. Miyazaki, "Stability and robustness of PID feedback control for robot manipulators of sensory capability," *International Symposium on Robotics Research*, pp. 783-799, 1983.

[5] R. Kelly and R. Carelli and O. Nasisi and B. Kuchen and F. Reyes, "Stable visual servoing of camera-in-hand robotic systems," *IEEE/ASME Trans. on Mechatronics*, Vol. 5, No. 1, pp. 39-48, 2000.

[6] J. J. E. Slotine and W. Li, "On the adaptive control of robot manipulators," *Int. J. Robot. Res.*, No. 6, pp. 49-59, 1987.

[7] C. C. Cheah and C. Liu and J. J. E. Slotine, "Adaptive tracking controls for robots with unknown kinematics and dynamic properties," *The International Journal of Robotics Research*, Vol. 25, No. 3, pp. 283-296, 2006.

[8] C. C. Cheah, C. Liu and J.J.E. Slotine, "Adaptive Vision based Tracking Control of Robots with uncertainty in Depth Information", *Proc. of IEEE Int. Conference on Robotics and Automation*, (Rome, Italy), pp 2817-2822, 2007.

[9] Y.H. Liu, H. Wang, C. Wang and K.K. Lam, "Uncalibrated visual servoing of Robots using a depth-independent interaction matrix", *IEEE Transactions on Robotics*, Vol. 22, No. 4, pp 804 - 817, 2006.

[10] S. Hutchinson, G. Hager and P. Corke, "A tutorial on visual servo control," *IEEE Trans. on Robotics and Automation*, vol. 12, no. 5, pp. 651 – 670, 1996.

[11] C. C. Cheah and J. J. E. Slotine, "Task-space Setpoint Control of Robots with Dual Task-space Information," *IEEE Int. Conference on Robotics and Automation*, (Kobe, Japan), pp. 3706-3711, May 2009.

[12] F. L. Lewis, C. T. Abdallah, and D. M. Dawson, *Control of Robot End-effectors*. New York: Macmillan Publishing Company, 1993.

[13] L. E. Weiss, A. C. Sanderson and C. P. Neuman, "Dynamic sensor-based control of robots with visual feedback," *IEEE Trans. on Robotics and Automation*, Vol. RA-3, No. 5, pp. 404-417, 1987.

[14] B. Espiau and F. Chaumette and P. Rives, "A New Approach to Visual Servoing in Robotics," *IEEE Trans. on Robotics and Automation*, Vol. 8, No. 3, pp. 313-326, 1992.

[15] J. J. E. Slotine and W. Li, *Applied Nonlinear Control*. Englewood Cliffs, New Jersey: Prentice Hall, 1991.

[16] C. C. Cheah and D. Q. Wang and Y. C. Sun, "Region-Reaching Control of Robots," *IEEE Trans. on Robotics*, Vol. 23, No. 6, pp. 1260-1264, 2007.

[17] http://www.hamamatsu.com